

Geometry calibration for X-ray equipment in radiation treatment devices

B. P. Selby & G. Sakas

Cognitive Computing and Medical Imaging, Fraunhofer IGD, Darmstadt, Germany

S. Walter

Medical Imaging, Medcom GmbH, Darmstadt, Germany

U. Stilla

Photogrammetry and Remote Sensing, Technische Universitaet Muenchen, Muenchen, Germany

ABSTRACT: It is essential for radiological tumor treatment to position a patient very accurate in the treatment device. To avoid sub-millimetre misalignments for a patient in the treatment facility, X-ray images acquired from within the device can be compared to the planning CT. But as slight displacements of the treatment beam nozzle, the digital X-ray panels and the X-ray tubes may arise over time and with movements of the dynamic parts of the treatment device, the underlying geometry model for the patient set-up correction may become inaccurate. To solve this problem, an automatic calibration routine is proposed, which bases on the known geometry of a calibration phantom and X-ray images acquired during the calibration routine. The result from the registration of the X-ray projections of the phantom and its known geometry is used to update the geometric model of the respective beamlines to enable accurate alignment correction.

1 INTRODUCTION

A great percentage of tumor diseases can be treated by the application of radiological doses onto the diseased tissue. To destroy carcinogen cells and to save surrounding tissue it is necessary to direct the treatment beam exactly onto the radiation target. Today, especially particle beam treatment techniques allow a very high accuracy of less than 1 mm and patient fixation equipment even assures set-up preciseness for the patient of less than 0.5 mm (Verhey et al. 1982). To avoid misalignments of the patient in the treatment device, a positioning fine-tuning is done by manual step-by-step correction, reducing the remaining offsets between a reference CT and X-ray images acquired from within the treatment device (Heufelder et al. 2004).

This procedure causes inaccuracies, which cannot be eliminated if the geometric model for the X-ray beamlines is not defined properly or if it is not up-to-date. Especially common systems that use X-ray flat panels mounted in a rotating gantry that delivers the particle beam suffer from this problem, because distortions of the gantry from the weight of the beam nozzle or misplacements of the flat panels from a flap-in and flap-out procedure cause geometric changes that affect the projection of the X-ray images and therewith lead to incorrect patient alignment corrections.

To overcome this problem, the geometric model for the imaging equipment of the treatment device should be re-calibrated frequently. In this

contribution an approach is presented, that allows an automatic image based calibration of the geometry model of the X-ray imaging devices. The modified model parameters are then taken into account for the treatment position set-up correction procedure.

2 STATE OF THE ART

During assembly of the treatment facility, the X-ray equipment is installed inside the rotatable gantry. The flat panels are either located on a special mounting or directly mounted to the beam delivery nozzle. In either case the geometric set-up can be determined via laser tracking systems, which gives an acceptable initial geometric definition of the system, but does not take any displacements into account that occur during lifetime of the machine.

Today, the periodic quality control for the geometric set-up of the imaging devices inside the treatment facility does not include a phantom based verification of the X-ray equipment (Dunscombe et al. 2007).

To track the displacement of the isocenter of an X-ray beamline, it is common practice to place a crosswire in front of the respective X-ray tube. With each acquisition, the wire is projected onto the X-ray panel and becomes visible in the image. An offset of the intersection point of the wires and the centre of the image indicates a displacement of the isocenter and can be evaluated after each image acquisition. The disadvantage of this procedure is, that it is not

possible to identify image distortions resulting from a flat panel rotation or a tube movement. Despite that, the crosswire leads to unwanted artefacts in the X-ray images.

To overcome these problems, we propose an automatic calibration on a regular basis that allows adjusting the geometric model of the X-ray systems and therewith increases the accuracy of the patient alignment. The procedure does not lead to any modifications of the X-ray images themselves.

3 METHODS

The refinement of the X-ray geometry definition involves several working steps during a calibration session:

- Manual alignment of the phantom on the treatment table
- Acquisition of X-ray images for several different gantry angles and snout positions
- Automatic calculation of corrections for the X-ray beamline geometry

During a treatment session the corrections for the X-ray beamline geometry are applied to the initial beamline model M_0 .

3.1 Description of parameters for the X-ray geometry

The X-ray tube and the X-ray flat panel define an X-ray beamline. The geometric set-up of the X-ray beamline is described by Model M_0 , which contains:

- Position of the X-ray tube
- Position of the X-ray panel
- Normal Vector of the panel plane
- Vector in Panel Y-direction

Depending on if the X-ray equipment is mounted to the rotating gantry or if it is positioned at a static position in the treatment room, the respective coordinate systems of the tube and the panel are defined in a gantry coordinate system or a fixed reference system.

3.2 Layout and positioning of the phantom

The phantom used for the calibration is a glass cylinder containing 26 gold spheres each with a diameter of 1.5 mm that have a high absorption coefficient for X-ray beams (see Fig. 1).

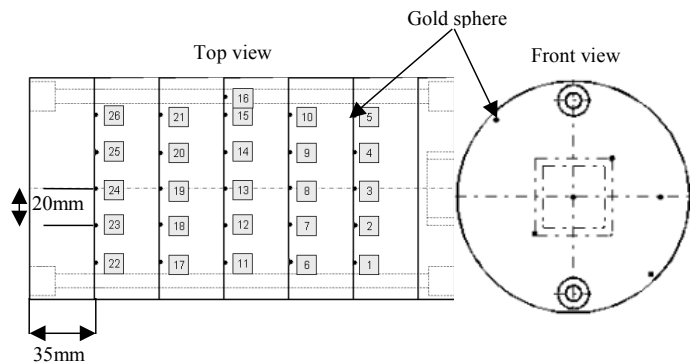


Figure 1. Schematic view of a calibration phantom. Seen from top (left) and from front (right).

The spheres are numbered from 1 to 26, whereas sphere 13 is the central sphere.

The phantom is positioned manually on the treatment table, so that the central sphere is located at the isocenter of the treatment device, which is, in the optimal case, the rotation centre of the gantry. To align the phantom properly on the tabletop in the device, a laser system is used (see Fig 2).

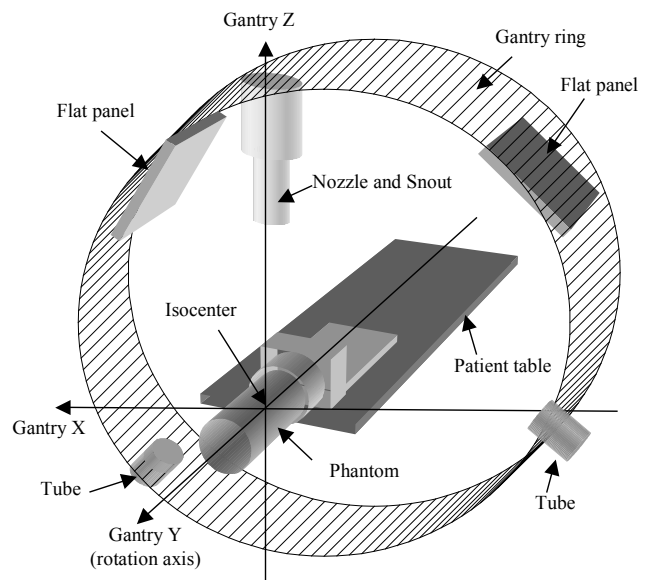


Figure 2. Placement of the phantom.

3.3 Image acquisition for the calibration process

If the X-ray equipment is mounted to the rotating gantry, one image per beamline has to be acquired for several gantry angles, for example in steps of 10° degrees of gantry rotation. As the alignment of the equipment can vary in dependence of the rotation direction, each angle is calibrated for a clockwise and a counter-clockwise rotation.

If the system has a movable snout for the treatment beam, the calibration should be done for several snout positions, as the treatment table may be realigned automatically for the treatment beam isocenter and herewith affects the alignment of the calibration phantom.

In total, the calibration of one beamline affords one image for one set of:

- Gantry angles with clockwise rotation,
- gantry angles with counter-clockwise rotation,
- snout positions

For each image one correction can be computed which modifies the initial beamline model according to the mapping in 1:

$$M'_{\alpha,d,sn} \xleftarrow{C_{\alpha,d,sn}} M_0 \quad (1)$$

where M' is the corrected beamline model, C is the correction, α is the respective gantry angle, d is the rotation direction and sn is the snout position.

3.4 Automatic calculation of corrections for a beamline model

The correction $C_{\alpha,d,sn}$ for one beamline is determined by projecting a model of the known phantom geometry onto the respective panel plane and then calculating the modifications to the initial beamline model that allow a mapping of the projected phantom model spheres P' onto the real X-ray image spheres P for the device configuration (α, d, sn) . Therefore the spheres P are detected in the X-ray images and are registered with the projected positions P' (see Fig. 3).

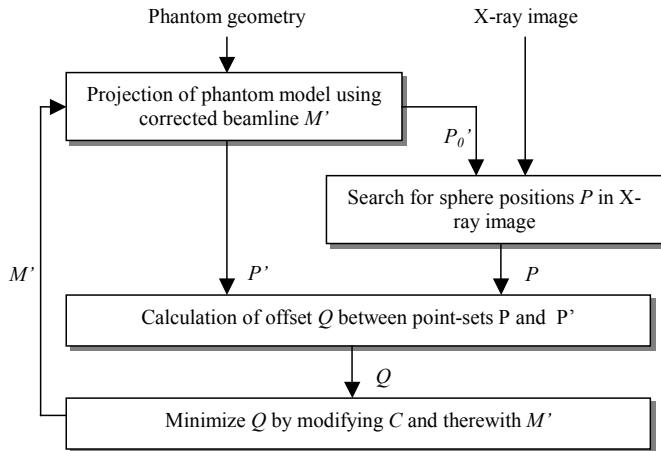


Figure 3. Calculation of a correction

3.4.1 Projection of the model of a phantom

As the locations of the spheres in the phantom are known, they can be projected into an X-ray panel plane, according to a corrected beamline model $M_{\alpha,d,sn}$ (see Fig. 4).

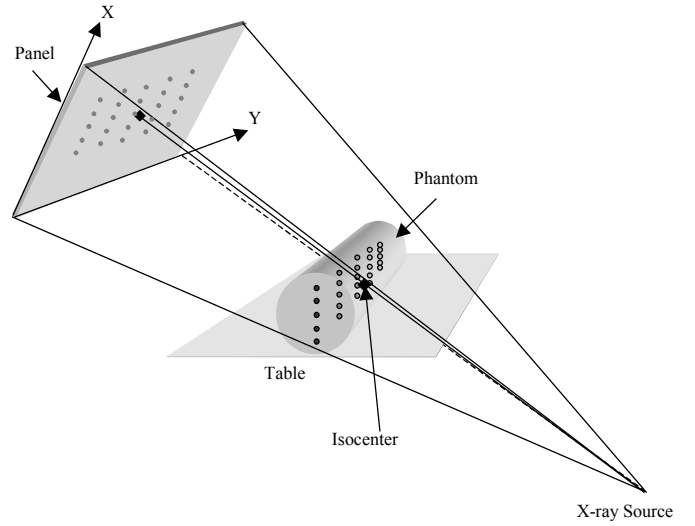


Figure 4. Projection of the phantom.

The geometric correction C applied to the initial beamline model M_0 consists of:

- Tilt around the X- and Y-axes of the panel
- Rotation around the normal vector of the panel
- Movement of the panel in X-, Y-axis and normal direction
- Movement of the X-ray tube in X-, Y- and Z-direction

The resulting coordinates of spheres in the plane of the flat panel depend on the position of the X-ray tube and the position and alignment of the panel. The resulting coordinates are given by the intersection point of a ray from the X-ray source through the respective sphere and the panel plane. They are defined in 2D space.

3.4.2 Detection of sphere positions in X-rays

The spheres appear as disks of high grey value intensity in the X-ray image (see Fig. 5).

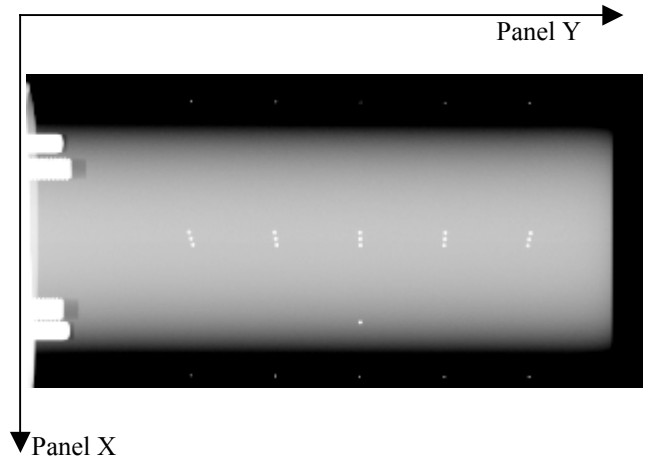


Figure 5. X-ray image of phantom.

Equation 2 gives the radius R of such a disk in the X-ray image:

$$R_{disk} = R_{sphere} * \frac{|\vec{V}_{disk}|}{|\vec{V}_{sphere}|} \quad (2)$$

where V_{disk} is the vector from the X-ray source to a projected disk and V_{sphere} is the vector to a sphere.

The goal of the detection procedure is to find the centres P of the spheres in an X-ray image. Detection of a single disk is hardly possible because of artefacts in the image, which can result for example from the mounting of the phantom. For this reason, the detection procedure for each disk is performed nearby the positions of the projected phantom model P' .

For each pixel in a distance of ± 15 mm nearby a point of P' , a value S is calculated by equation 3:

$$S = \sum_{i=-R-1}^{R+1} \sum_{j=-R-1}^{R+1} (I(x+j, y+i) * k(x+j, y+i)) \quad (3)$$

$$k = \begin{cases} +1 & \text{for } j^2 + i^2 \leq R^2 \\ -1 & \text{else} \end{cases}$$

where R is the radius of a disk in pixels and I the intensity of a pixel. For each point of P' a maximum for S can be found, which determines the location x and y of the respective disk centre of P .

3.4.3 Registration of the phantom model and the X-ray image

After the spheres of the phantom model have been projected computationally into the panel plane and the disk centres in the X-ray image have been found, the next step is to find the correction C for the initial beamline model that minimizes the offset between the spheres in an X-ray image of the phantom and the projected model of the phantom (see Fig. 6).

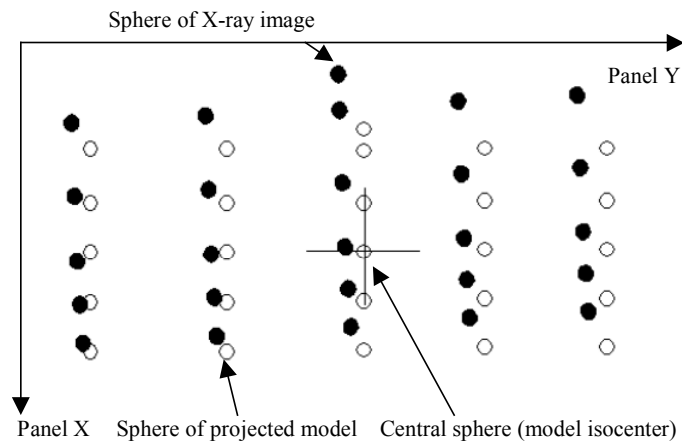


Figure 6. Spheres of phantom model and real X-ray projected into plane of the X-ray flat panel.

The transformation between the 2D point-sets is a non-rigid transformation. It is caused by the misalignment of the X-ray equipment in 3D space.

To minimize the offset between the positions, a downhill simplex algorithm is used (Teukolsky et al.

1992), which minimizes the squared distances between the projected points of the model and the X-ray image as shown in equation 4:

$$Q = \sum_{i=1}^{26} ((x_i' - x_i)^2 + (y_i' - y_i)^2) \quad (4)$$

where Q denotes the value to minimize, i is the index for a sphere, x' and y' are the coordinates of the projected phantom spheres P' and x and y are the centres of the disks P in the X-ray image.

The optimisation is done in 9 dimensions, to find all 3 panel rotations, 3 panel shifts and 3 tube shifts at once.

After one pass of the optimisation procedure, a remaining error Q indicates how good the beamline model M_0 could be corrected. The impact of the largest error Q_{imp} on the patient alignment is estimated by equation (5):

$$Q_{imp} = \sqrt{\max_i ((x_i' - x_i)^2 + (y_i' - y_i)^2)} * \frac{|\vec{V}_{Ri'}|}{|\vec{V}_{Pi'}|} \quad (5)$$

where $V_{Pi'}$ is the vector from the beam source to the projected point with the maximal error and $V_{Ri'}$ is the vector to the corresponding point of the phantom in 3D space of the treatment room. If the error value exceeds a certain threshold of for example 1 mm, the algorithm tries to redetect the respective disk in the X-ray image, assuming, that starting detection at a refined position, generated through beamline model M' , the result becomes more accurate. After a new detection, the registration is resumed.

The final result is obtained, as soon as the maximal error value falls below the threshold, or no improvement could be achieved by repetition.

3.5 Application of the adjusted geometry model in treatment sessions

During the calibration, a number of corrections have been calculated, that transform an initial beamline M_0 into a corrected beamline $M'_{a,d,sn}$. During the treatment of a patient, the relevant values to select the correct beamline model for the patient alignment correction are gantry angle α , rotation direction d and snout position sn . The gantry angle and the snout position are provided by the treatment plan (DICOM 2006). This is not the case for the rotation direction of the gantry, which may rotate in any direction to arrive at the proper angle.

In order to obtain the best model M' for the given treatment situation, first the nearest gantry angles α_0 and α_1 for a current angle α are determined from the list of calibrated angles, so that $\alpha_0 \leq \alpha \leq \alpha_1$.

Then the following sets of corrections are chosen: $C_{a0,CW(sn)}$, $C_{a0,CCW(sn)}$, $C_{a1,CW(sn)}$ and $C_{a1,CCW(sn)}$, where C is a set of corrections for all snout positions

sn and CW or CCW denotes the rotation direction clockwise or counter-clockwise.

From each set of corrections, the two existing corrections for a snout position sn_0 and sn_1 near to the current snout position are selected so that $sn_0 \leq sn \leq sn_1$. Now the correction values of each of the 8 corrections C_{α_0, CW, sn_0} , C_{α_0, CW, sn_1} , C_{α_0, CCW, sn_0} , ..., C_{α_1, CCW, sn_1} are interpolated.

For the gantry angles and the snout positions we use bilinear interpolation as in equation 6:

$$C_{\alpha, sn} = \sum_{i=0}^1 \sum_{j=0}^1 C_{\alpha_i, sn_j} * w_{\alpha_i, sn_j} \quad (6)$$

with

$$w_{\alpha_i, sn_j} = \frac{|\alpha - \alpha_i|}{\alpha_1 - \alpha_0} * \frac{|sn - sn_j|}{sn_1 - sn_0} \text{ and } \sum_{i=0}^1 \sum_{j=0}^1 w_{\alpha_i, sn_j} = 1$$

We obtain two corrections, one for each rotational direction of the gantry. Our final correction that is applied to the initial beamline model M_0 is the average of these.

4 RESULTS

Tests have been performed in three different gantry constructions:

1. System with rotatable gantry but static panels mounted in treatment room
2. System with flat panels mounted to a nozzle in a rotatable gantry
3. System with panels in a rotatable gantry with movable snout

A phantom with 26 gold spheres was used for the tests (see Fig. 7)

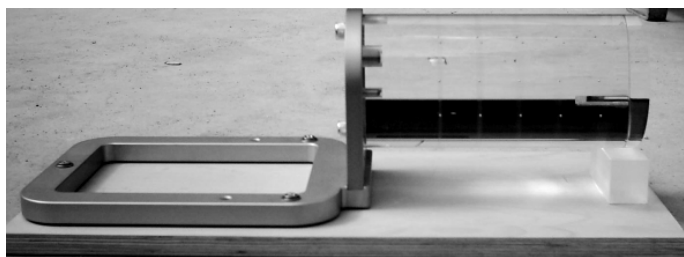


Figure 7. Photography of a calibration phantom.

In the first test scenario the calibration has been performed for only one gantry angle, as the flat panels were fixed in the room. Nevertheless, aberrations of the initial beamline geometry could be determined during the calibration session. The maximum aberration was a tube shift of 12.5 mm. After the calibration we simulated a treatment situation, using a patient phantom. Before the calibration, the remaining alignment error for the patient was 3.1 mm. After the calibration we could

achieve alignments with accuracy better than 0.5 mm using the X-ray equipment.

The set-ups with moving X-ray devices have been calibrated for gantry angles in 45° steps clockwise and counter-clockwise. In the case of the movable snout, we used snout movements in steps of 25 mm.

In both cases, the initial geometric set-up of the systems were misaligned by more than 25 mm for the tubes and about 18 mm shift and 0.8° normal rotation for the panels (see Fig. 8).

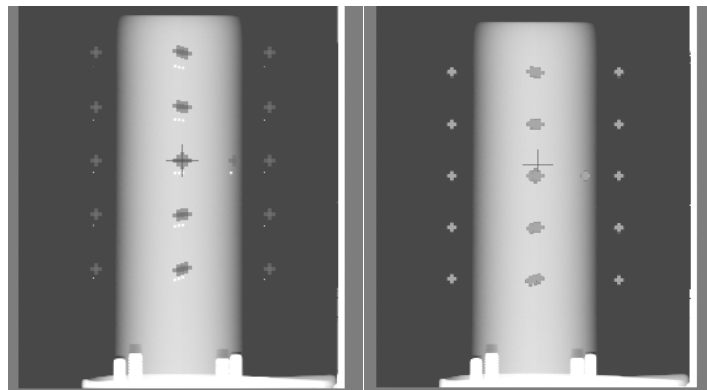


Figure 8. Projection of phantom model onto misaligned X-ray (left) and projection after the alignment correction (right).

Movement of the snout did affect the beamline alignment in less than 1.0 mm, but gantry rotations of 45° caused alignment deviations of maximal 7 mm and 0.8° for the panels and 10 mm for the X-ray tubes. Differences between clockwise and counter-clockwise rotations caused variations in the panel shift of a maximum of 2.0 mm.

Before the calibration the maximal error for the best patient set-up was 8.7 mm. After the calibration routine the maximal alignment error was 0.9 mm.

The calculation time for the calibration of one beamline at one specific gantry angle and snout position varies between 10 and 20 seconds on a standard PC, depending on the offset between the initial beamline geometry and the real geometry. This results in a total calibration time of up to 1:45 h for 8 gantry angles in both directions, two beamlines and 10 different snout positions, without the time needed for the image acquisition.

5 CONCLUSIONS

Through the geometry calibration of the beamlines the accuracy for the patient alignment could be raised dramatically, whereas the initial set-up of the geometry is often unacceptable if alignments with less than 0.5 mm error have to be achieved. The automatic alignment procedure proposed in this contribution could reduce the patient alignment errors and can additionally serve as an indicator for the initial accuracy of the beamline installation.

The relative high time exposure for the calibration is noncritical because the calibration is not done during the treatment session and can be conducted during a regular quality validation of the treatment device.

It would be possible to reduce the remaining errors after the calibration (maximum 0.9 mm) if:

- More gantry angles and snout positions would be used
- Information about the rotation direction of the gantry for a specific treatment set-up could be provided to the application
- A larger phantom would be used, as distortions are mainly visible as offsets of the outer spheres. A candy cane type phantom could increase the accuracy (Claus 2006)
- A method more suitable for the initial alignment of the calibration phantom on the treatment table than the laser alignment system could increase the accuracy of the final calibration result

REFERENCES

- Claus, B. E. H. 2006. Geometry calibration phantom design for 3D imaging. *Physics of Medical Imaging* 6142: 823-834.
- DICOM 2006. *Digital Imaging and Communications in Medicine Part 3*. Rosslyn: National Electrical Manufacturers Association.
- Dunscombe, P. et al. 2007. Development of quality control standards for radiation therapy equipment in Canada. *Journal of applied clinical medical physics* 8(1): 108-118.
- Heufelder, J. et al. 2004. Fuenf Jahre Protonentherapie von Augentumoren am Hahn-Meitner-Institut Berlin. *Zeitschrift fuer Medizinische Physik* 14: 64-71.
- Teukolsky, S. A. et al. 1992. *Numerical Recipes in C*. Cambridge: Cambridge University Press.
- Verhey, L. J. et al. 1982. Precise positioning of patients for radiation therapy. *International Journal of Radiation Oncology* 8(2): 289-294.